Tellus (1997), 49A, 439–454
Printed in UK – all rights reserved

TELLUS
ISSN 0280–6495

High-latitude cold season frontal cloud systems and their precipitation efficiency

By K. K. SZETO[1]*, R. E. STEWART[1] and J. M. HANESIAK[2], [1]Atmospheric Environment Service, Downsview, Ontario, Canada; [2]Department of Geography, University of Manitoba, Winnipeg, Manitoba, Canada

(Manuscript received 2 August 1996; in final form 11 April 1997)

ABSTRACT

A weak high-latitude warm-frontal precipitation system was simulated by using a 2D cloud-resolving model. It was found that many of the structural characteristics of the system were consequences of the subfreezing temperatures and enhanced planetary rotation in the region. The coupling of cloud microphysical processes to frontal scale dynamics caused the precipitation efficiency (defined as the ratio of integrated surface precipitation rate to the net water vapor influx into the storm) of the model storm to exhibit strong sensitivity to low-level humidity conditions. A relatively high (zero) precipitation efficiency is associated with a storm if it develops over regions having near surface relative humidity with respect to ice $\geqslant(<)$ 80%. In addition, the model results show that the precipitation efficiency of a system is decreased (increased) when the background static stability is increased (decreased) or when the Coriolis parameter is increased (decreased). These model results may have great implications for the Arctic water cycle as well as for the parameterization of Arctic clouds and precipitation in GCMs.

1. Introduction

It is well-known that earth's climate system is very sensitive to changes in Arctic surface conditions. First, there is a large storage of water (in the form of snow and ice) in the region. Second, most climate model results suggest that the positive feedback between air temperatures, ice extent and surface albedo in the polar region is critical to the global energy balance (Washington and Meehl, 1996). Both aspects of the global climate system depend critically on the amount of snow that falls over the Arctic region. In addition, the local distribution of water vapor, which is the most abundant greenhouse gas in the atmosphere, also depends significantly on the characteristics of the cloud systems occurring over the region. To improve our understanding of the Arctic environment and its subsequent impacts on the global water and energy cycles, we must improve our knowledge of the synoptic cloud systems that produce much of the precipitation over the region in the first place.

Most recent investigations of high-latitude cloud systems have concentrated on polar low systems or comma cloud systems which occur over the (relatively) warm open sea where sufficient energy in the form of latent and sensible heat is available to drive the systems (Grønås et al., 1987; Nordeng, 1990). Comparatively, our knowledge of synoptic storms which occur over the frozen or solid surfaces has been very limited although a number of studies on the internal structure of such systems have been conducted over northern Europe (Saarikivi, 1990; Saariviki and Puhakka, 1990).

* Corresponding author address: CCRP, AES, 4905 Dufferin Street, Downsview, Ontario, M3H 5T4 Canada. e-mail: kit.szeto@ec.gc.ca.

The Arctic environment has several unique characteristics that might have great impacts on the storms that develop over or move into the region. First, planetary rotation and thus the background inertial stability is strong. Second, due to the prevailing sinking motion under the semi-permanent Arctic high pressure systems (Stewart et al., 1995a) and cold (frozen) surface in the region, static stability is typically strong in the lower troposphere during the cold season. Therefore, high-latitude synoptic systems are generally shallow and have small horizontal scales. Third, surface temperatures are typically below 0 °C from the late fall through the winter till spring. Consequently, snow is the dominant form of precipitation in the region during much of the year. Sublimation rather than evaporation will then be the main sink for the condensate produced in these storms. Fourth, the low level moisture supply can be limited due to the cold temperatures and frozen water surface. Therefore, the amount of precipitation from the Arctic synoptic systems is typically small. However, since almost all of the precipitation falls in the form of snow and remains on the surface in solid form, very little is lost by runoff. As such, the amount of snow produced by the storms plays a very crucial role in controlling the water budget in the region.

To improve our understanding of the nature of these systems, the Beaufort and Arctic Storms Experiment (BASE) was conducted over the Canadian Arctic during the fall of 1994. Several synoptic systems were observed by using surface and air-borne instruments during the experiment. In this study, we will examine the structure of a warm-frontal precipitation system observed during the BASE period. A detailed observational study of the system is given in Hanesiak et al. (1997). In the present paper, the development of the system is investigated with the aid of a 2-D numerical cloud model. In particular, the effects of the environmental conditions and cloud processes on storm development and storm water budget will be investigated. A special emphasis will be placed on the precipitation efficiency (PE, defined as the ratio of horizontally integrated surface precipitation flux to the net moisture influx into the storm region).

A brief summary of the observed frontal system will be given in the next section. A description of the numerical cloud model used in this study will be given in Section 3. Results of the simulations will be presented in Section 4 while a discussion of the model results and concluding remarks will be given in Sections 5 and 6, respectively.

2. Observations

A detailed analysis of the warm frontal system is given in Hanesiak et al. (1997) and only a brief summary of the case will be presented here. The warm front investigated in this study was associated with the last of three disturbances embedded in the strong upper west northwesterly flow over the region during late September of 1994. The parent low-pressure system had started to occlude by the time it passed over the southern Beaufort Sea. At ~2100 UTC 30 September 1994, the National Research Council Convair 580 research aircraft flew through the warm-frontal zone measuring the standard thermodynamic variables, horizontal and vertical winds, cloud and precipitation particles. Several dropsondes were released at different stages throughout the flight to supplement the aircraft data.

The temperature and humidity fields across the front are shown in Fig. 1. The storm environment is characterized by sub-freezing temperatures and a relatively weak and steep warm frontal zone is evident in the temperature field. The average

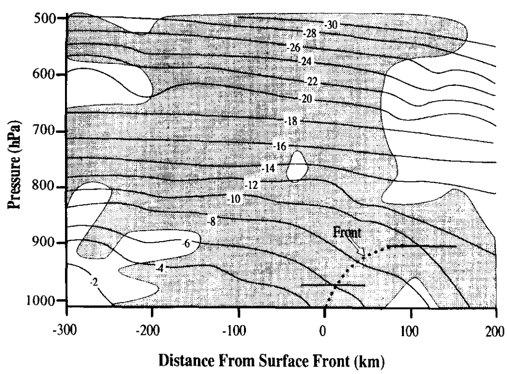

Fig. 1. Vertical distribution of temperature (°C) as a function of distance from the surface warm front. The shaded area is characterized by relative humidity >95% (w.r.t. ice). The location of the low-level warm front is indicated by a dashed line and the two thick lines through it indicate the low-level horizontal aircraft flight tracks. (Adapted from Hanesiak et al., 1997).

horizontal temperature gradient across the enhanced baroclinic zone was about 3K/100 km. It is also evident that the horizontal scales of the overall frontal structure and the associated cloud field were small. Near-saturated conditions (with respected to ice) extended from the surface to about 500 hPa. A mid-level dry air intrusion occurred about 80 km ahead of the surface front.

It is of interest to note that a substantial portion of the cloud and precipitation occurred in the warm sector, contrary to some observed mid-latitude systems where the precipitation occurs mostly ahead of the surface warm fronts and the cloud base rises sharply following frontal passages (see for example the observations of mid-latitude frontal systems by Stewart et al., 1995b). The cloud deck consisted mainly of ice particles with only a minute amount of cloud liquid water near the frontal zone. Precipitation was light and fell exclusively in the form of snow. The maximum snowrate was less than 0.2 mm h^{-1} and this was located near the surface front. Due to the saturated conditions throughout the low levels, sublimation of snow was negligible in the immediate vicinity of the surface front. Despite the extremely light precipitation that was falling from this system, a rather high precipitation efficiency of $\sim$60% was estimated from the data (Hanesiak et al., 1997). This value of PE is comparable to those estimated for some mid-latitude frontal precipitation systems ($\sim$60–90% from Houze et al., 1976; $\sim$70% from McBean and Stewart, 1991) while considerably higher than those associated with some other observed frontal systems ($\sim$20%, Hobbs et al., 1980; Carter and Long, 1995).

The overall frontal circulation (not shown) was weak. The lower levels were characterized by weak upward motion across the frontal zone. A low-level along-front jet with maximum velocity $\sim$15 m s^{-1} was located just to the cold side of the surface front and (system relative) cross-front velocities in the low-to-mid levels were typically less than 10 m s^{-1}.

The observations presented herein reveal several interesting and important characteristics of the mature high-latitude warm-frontal system. In particular, a relatively high PE was associated with this system despite its overall weak structure. It is of interest to investigate how these characteristics of the system developed during the life-cycle of the storm. We are also interested in knowing the generality of these observed characteristics among the Arctic winter synoptic storms, i.e., the sensitivity of the storm characteristics to environmental conditions. Unfortunately, observations of the system during its earlier stage of development were not available. To gain insights on these aspects of the observed frontal system, a numerical cloud model has been used.

3. Model description and experimental design

3.1. Model description

The 2-D, nonhydrostatic and anelastic cloud model of Szeto and Cho (1994) is adapted for use in the present study. Homogeneous conditions (except the large-scale horizontal temperature gradient) are assumed for the variables in the along-front direction. Frontogenesis in the model is forced by both idealized large-scale confluence and shearing deformation. A time-dependent basic-state solution corresponding to this kind of frontogenetic forcing as devised by Keyser and Pecnick (1985, 1987) is used to simplify the model equations. A simple 1st-order closure scheme adapted from Deardorff (1971) using the local deformation field (along with a base eddy exchange coefficient of 1.5 m^2 s^{-2}) to determine the eddy viscosity and diffusivity is employed throughout the whole domain. Radiational effects and surface friction are neglected in these simulations. Free-slip conditions are used at the surface and at the model top while open conditions are used at the lateral boundaries.

The bulk water cloud microphysical parameterization scheme used in Szeto and Cho (1994) is modified to represent more accurately the conditions in large-scale frontal precipitation systems (see Szeto and Stewart, 1997). The formulation of the scheme is similar to that of Rutledge and Hobbs (1983). Prognostic variables for 6 types of water substance (water vapor, cloud droplets, cloud ice, snow, graupel and rain) are considered in the parameterization. Microphysical processes considered in this scheme include evaporation/condensation, deposition/sublimation, melting/freezing, coalescence, accretion, riming and growth. Condensation and evaporation are treated as isenthalpic processes (see for example, Rutledge and Hobbs, 1983). The autoconversion of cloud water (ice) to rain (snow) is treated using the

Kessler (1969) approach. The (temperature-dependent) concentration of ice nuclei is assumed to follow the Fletcher (1962) formula. The growth/depletion of ice-phase particles by deposition/sublimation are calculated with diffusion-controlled kinetic formulae. Melting and freezing of precipitation are not important in the type of systems studied here. Further details of the cloud scheme can be found in Cho et al. (1989).

The simulations were performed on a $7680\ \text{km} \times 10\ \text{km}$ domain with $\Delta x = 7.5$ km and $\Delta z = 250$ m. All integrations are carried out to 70 hours with a timestep of 14 s. Further details of the numerical model can be found in Szeto and Cho (1994) and Szeto and Stewart (1997).

3.2. Experimental design

Due to the limitation and formulation of the present 2-D frontal model, initialization by using observed conditions is difficult. For example, the initial cross-front flow must have constant vertical shear in order to satisfy the 2-D requirement. Therefore, idealized environmental conditions are used in the present simulations to simplify the interpretation of the results. Frontal forcing in all cases consists of an externally maintained background deformation flow (with the confluence parameter α set at $4 \times 10^{-6}\ \text{s}^{-1}$) and a time-dependent along-front temperature gradient in thermal wind balance with the basic cross-front flow. The initial vertical shear of the cross-front flow is $1.5 \times 10^{-3}\ \text{s}^{-1}$ corresponding to an initial along-front horizontal temperature gradient of -6.1×10^{-1} K/100 km. These rather weak forcings (as compared to those used in some simulations of midlatitude frontal systems, e.g., Keyser and Pecnick, 1987; Szeto and Stewart, 1997) are estimated from the results of a 3-D nowcasting simulation of the system performed by using the MC2 mesoscale model (Tanguay et al., 1990). The basic along-front temperature gradient (and the associated vertical shear of the basic cross-front wind) will decay exponentially with an e-folding time given by $1/\alpha$ (~ 70 h). This time-dependency of the along-front temperature gradient is a consequence of the stretching in the along-front direction by the basic deformation flow (see Keyser and Pecnick, 1985). An initial baroclinic disturbance consisting of a weak tropospheric front-jet system is placed in the middle of the domain (Fig. 2).

Since the storm occurred over the Beaufort Sea which was only partially frozen in late September, a moist humidity condition at the lower levels was specified in the control simulation (CONTR). The initial humidity is specified with RH constant at 90% in the lowest 2 km, decreasing linearly to 50% at 5 km and then to 30% at the top of the domain (10 km). The initial θ lapse rate at the left (warm side) domain boundary was specified to be 2.5 K km^{-1} at the lowest km and 3 K km^{-1} at the higher levels. These θ lapse rates are estimated from the soundings observed in the warm sector of the storm (over land). The tropopause is specified at 8.5 km AGL which is similar to that observed in the region during the BASE period. The simulation was performed on a f-plane at 73°N.

Several experiments were performed to gauge the effects of different environmental conditions on the development of the cloud system (see Table 1). The effects of a smaller Coriolis parameter (f) were examined in experiment MID−LAT in which the simulation was performed on a f-plane at 45°N. The effects of stronger background static stability on the development of the model frontal precipitation system were examined in experiment MORE−STABLE where the initial θ lapse rate at the left domain boundary is set at 6.5 K km^{-1} throughout the troposphere. The sensitivity of the model storm to initial low-level moisture conditions was examined in experiments RH70–RH85 in which the relative humidity at the lowest 2 km is varied systematically from 70% to 85% (see Table 1). In addition, the sensitiv-

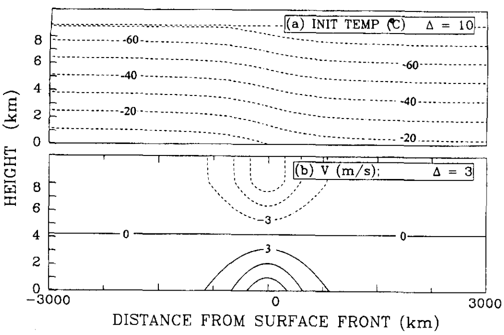

Fig. 2. Temperature (a) and the along-front velocity (b) at 0 h for the simulations.

Table 1. *Summary of model parameters used in the simulations*

Simulation	$f\,(10^{-4}\,s^{-1})$	Mid-level $\Delta\theta/\Delta Z$ (K/km)	Low level RH_o (%)	Cloud scheme
CONTR	1.33	3	90	full
MID−LAT	1.00	3	90	full
MORE−STABLE	1.33	6.5	90	full
RH70	1.33	3	70	full
RH74	1.33	3	74	full
RH77	1.33	3	77	full
RH80	1.33	3	80	full
RH83	1.33	3	83	full
RH85	1.33	3	85	full
MID−LAT−RH80	1.00	3	80	full
WARMRAIN	1.33	3	90	warm rain

ity of the model storm to a drier environment at lower latitudes was examined in a simulation (MID−LAT−RH80) where the Coriolis parameter is set at $1 \times 10^{-4}\,s^{-1}$ and the surface RH is set at 80%, respectively. The bulk effects of ice-phase microphysics on the model storm were examined in simulation WARMRAIN where all the ice-phase processes were switched off in the cloud scheme. All other background conditions for the sensitivity experiments are identical to those used in CONTR.

Finally, it should be noted that the problem is not strictly two-dimensional due to the assumed background along-front temperature gradient (i.e., the diabatic effects due to moist processes will not be homogeneous in the along-front direction). However, since the initial along-front temperature gradient used in the simulations is weak (<1 K/100 km) and it decays with time, it is reasonable to assume that the vertical circulation in the along-front plane induced by such effects will also be weak and negligible when compared to the corresponding effects in the cross-front direction.

4. Results

4.1. *The control case*

Under the action of large-scale frontogenetic forcing, the initial frontal zone develops slowly in the first 30 h of the simulation. Large-scale overturning occurs above the frontal zone which causes saturation in the mid-to-upper model troposphere. Trace amounts of snow fall out of the cloud deck but most of it is sublimated in the sub-cloud layer during the early stage of storm development. Appreciable amounts of snow reach the surface by about 35 h.

The time series of the maximum frontal contrast (defined here as the maximum value of $|\partial\theta/\partial x|$ within the model domain) is presented in Fig. 3. It can be noted that surface frontogenesis is first accelerated around 30 h and further enhancement begins around 45 h. Maximum frontal contrast at the end of the simulation is about 7 K/100 km.

The structure of the model storm at 30 h and

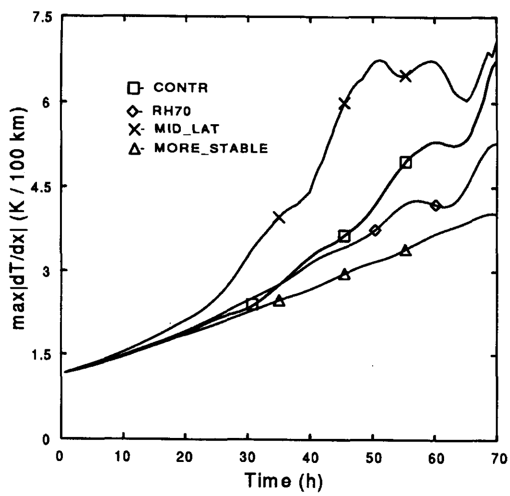

Fig. 3. Time series of the maximum horizontal temperature gradient in cases CONTR, RH70, MID−LAT and MORE−STABLE.

70 h is presented in Figs. 4, and 5, respectively. At 30 h, the surface frontal zone is still very weak and shallow (Fig. 4a). The associated cross-frontal circulation (Figs. 4b-c) is also very weak. The large-scale updraft is centered above the surface front. Consequently, the frontal cloud and precipitation fields are also distributed quite symmetrically about the surface front (Fig. 4d). Cloud top is near 5 km AGL. Sublimation of snow in the sub-cloud layers is evident in both Figs. 4d and 6a. The cooling from sublimational processes is located right at the region of surface frontal convergence and it therefore has a detrimental effect on the development of the frontal uplift.

By 70 h, the surface frontal zone is better defined and it has developed upward into the lower troposphere (Fig. 5a). The surface front is located near the $-4\,^{\circ}C$ isotherm and the overall thermal contrast across the enhanced baroclinic zone is about 3 K/100 km, similar to that in the observed system. A surface along-front jet (not shown) with magnitudes near 25 m s^{-1} is located just to the cold side of the surface front. The magnitude of this surface jet is somewhat stronger than that in the observed

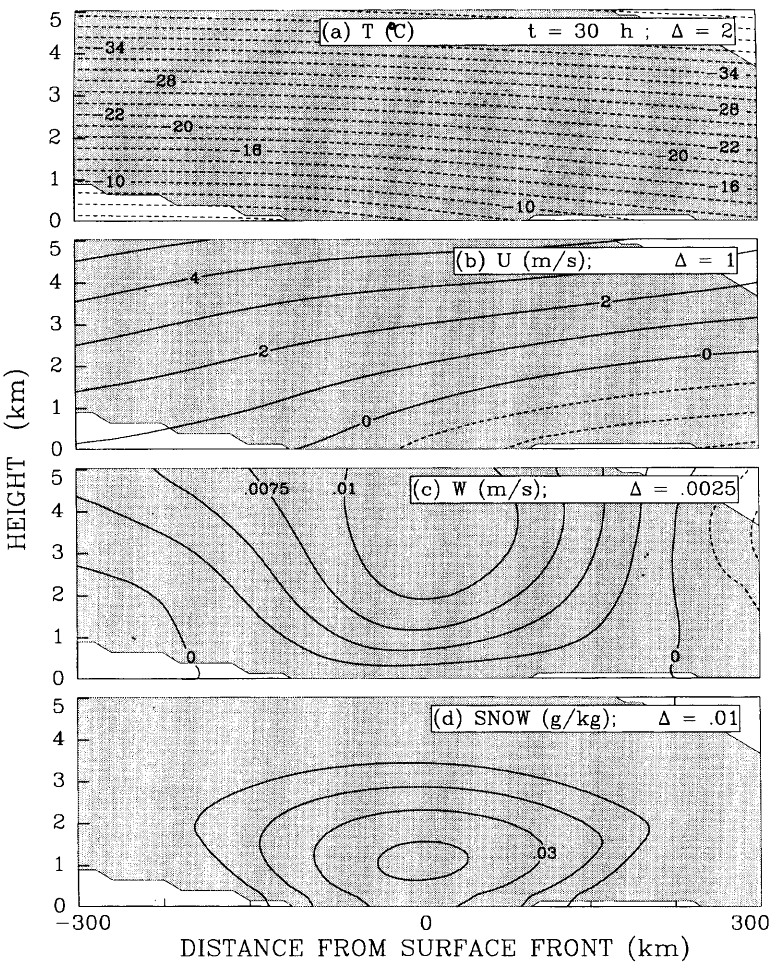

Fig. 4. Frontal structure at 30 h for the CONTR case: (a) temperature , (b) cross-front velocity, (c) vertical velocity and (d) snow mixing ratio. Shaded areas denote regions with relative humidity >95% (w.r.t. ice). Units and contour intervals are given in the label boxes.

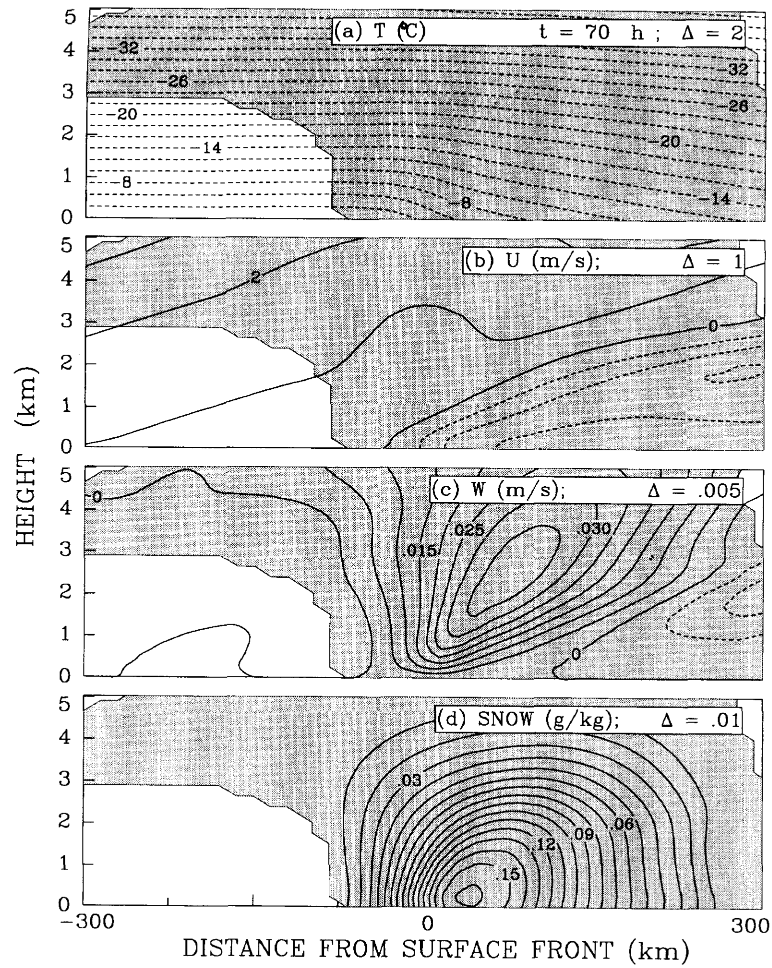

Fig. 5. As in Fig. 4 but at 70 h.

case (~ 15 m s^{-1}), presumably due to the use of free-slip surface conditions in the model. The cross-frontal circulation has also strengthened by this time (Figs. 5b-c). When compared to the model storm at 30 h, the horizontal convergence within the whole low level frontal zone has increased significantly. A mid-level dry intrusion from the cold side of the system is evident at $\sim$4–5 km altitudes and near $\sim$300 km from the surface front (Fig. 5b) but it is not as pronounced as that in the observed system (Fig. 1). The upward and forward development of the low-level frontal structure causes the frontal updraft to slope towards the cold side of the surface front (Fig. 5c). Consequently, the frontal cloud and precipitation fields are also shifted to the cold side of the surface front (Fig. 5d). Saturated conditions (with respect to ice) extend from the surface to about 6 km AGL and the snow mixing ratio at the surface has increased substantially when compared to the values at 30 h. The maximum surface snowrate is about 0.5 mm h^{-1}, roughly double that of the observed system although it should be noted that regions of higher precipitation may have been missed in the observations. Sublimational cooling at this time is insignificant and is mainly limited to the inflow region and around cloud edges (Fig. 6b).

Similar to the observed system, the model frontal system possesses a rather steep vertical

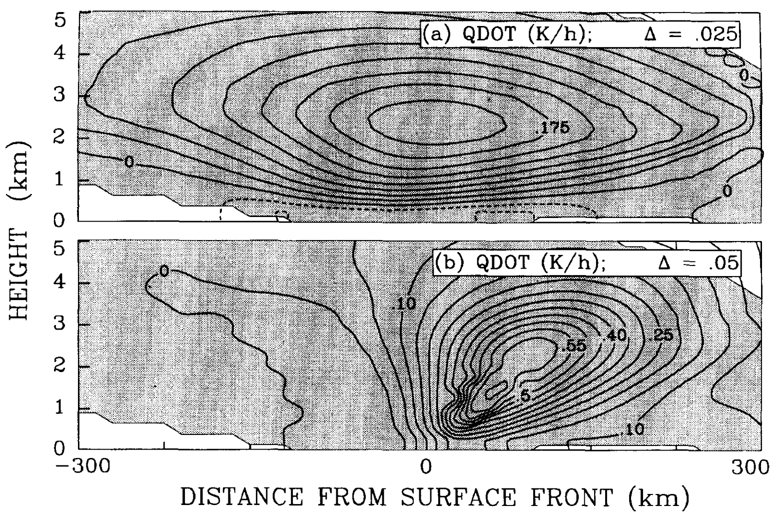

Fig. 6. Heating rates at (a) 30 h and (b) 70 h for the control case.

structure. The horizontal scale of the model storm is also comparable to that of the observed system. Both the observed and modelled frontal zones possess an average frontal slope of $\sim 1/100$ in the lowest kilometer.

The temporal evolution of the precipitation efficiency (PE, calculated as the ratio of horizontally integrated surface snowrate to the net moisture convergence into the storm region which has been taken to be the region ± 500 km from the surface front) of the model storm is given in Fig. 7. During the early stage of storm development when the frontal uplift is weak and the lower level is sub-saturated, the PE of the system is quite small. A significant amount of the snow is sublimated in the sub-cloud layer (Figs. 4d and 6a). The sublimation of snow moistens and cools the lower troposphere and saturates it by 45 h. It is of interest to note that surface frontogenesis accelerates considerably after this time (Fig. 3). The PE of the system also increases rapidly after that time and reaches a value of $\sim 70\%$ by the end of the simulation. The PE calculated for the observed system is about 60% which corresponds to the modelled value at about 50 h. The evolution of the model cloud and precipitation field also suggests that the observed system is best compared to the model storm at about 50 h.

In summary, the gross characteristics of the mature model storm compare quite well to those of the observed system. Therefore, the sensitivity of the weak Arctic system to variations in environmental conditions can be investigated with the model with some confidence and the results of these sensitivity studies are presented in the following sections.

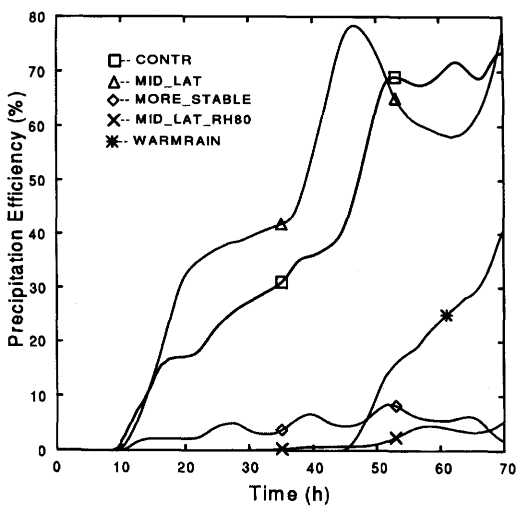

Fig. 7. Time series of the precipitation efficiency of the model storms in simulations CONTR, MID−LAT, MID−LAT−RH80, MORE−STABLE and WARMRAIN.

4.2. The "midlatitude" case

It is well-known that the cross-front ageostrophic circulation is essential to the rapid development of atmospheric fronts (Hoskins and Bretherton, 1972). Hence, any environmental factor that might enhance (suppress) the ageostrophic circulation will also enhance (suppress) frontogenesis. The vertical frontal ageostrophic circulation is given diagnostically by the Sawyer-Eliassen equation (see for example Bluestein, 1986). An analysis of the Sawyer-Eliassen equation suggests that if the inertial stability (proportional to fv, where v is the along front velocity) is small (large) compared with the static stability, the horizontal branch of the circulation would be enhanced (inhibited) while the vertical branch would be inhibited (enhanced) (Bannon, 1984). The model results from experiments MID−LAT and MORE−STABLE are in qualitative agreement with these theoretical predictions.

Surface frontogenesis is more rapid in the midlatitude (MID−LAT) case when compared to that in the control simulation (Fig. 3). An enhanced frontogenetic period occurs at ~ 39 h, slightly earlier than that in the control case. The quasi-steady maximum frontal contrast is also slightly stronger than that in case CONTR.

The structure of the model frontal system for case MID−LAT at 70 h is given in Fig. 8. The model frontal zone possesses a shallower slope when compared to that in the control case ($\sim 1/150$ versus 1/100). The weaker inertial stability in the environment of case MID−LAT allows the development of a stronger cross-frontal circulation than that in the control case. The more intensive cross-frontal circulation in the midlatitude case is reflected in the stronger vertical shear in the cross-front wind and the generally stronger frontal updraft (Figs. 8b-c). Associated with the stronger cross-frontal circulation in case MID−LAT is the larger horizontal scale of the model frontal structure. The wider horizontal scale of the system in this case is most evident in the cloud and precipitation features of the system (Fig. 8d). When compared to the control case, the model storm in case MID−LAT possesses a much more extensive cloud shield and a wider precipitation region. The region of maximum surface precipitation is also displaced further to the cold side of the surface front. Similar to the control case, saturation extends to the surface at the mature stage of the model storm and snow sublimation is not evident at 70 h.

The time series of the PE for the system is shown in Fig. 7. In accordance with the stronger frontal overturning in case MID−LAT, the PE is also generally higher in this case. Similar to the control case, the PE of the system increases rapidly following the saturation of the lower levels and the onset of the enhanced frontogenetic period (Fig. 3).

4.3. The "more stable environment" case

The model frontal system developed in case MORE−STABLE is significantly weaker than that in the control case (Fig. 3). In addition, unlike cases CONTR and MID−LAT, there is no enhanced frontogenetic period in this case and the surface frontal zone develops steadily but slowly under the large-scale forcing throughout the simulation period. Consequently, the storm structure (not shown) is significantly weaker in the present case. The enhanced background stratification in this case limits the magnitude of the frontal updraft and therefore the development of the cross-frontal circulation (Bannon, 1984). The resultant cloud shield is shallower and significantly less snow is produced than in the previous cases. Saturation never extends to the surface and a major portion of the snow is lost in the sub-cloud layer. These effects are reflected in the evolution of the PE for the system (Fig. 7). The PE of the system is less than 10% throughout the simulation.

Similar results are obtained from another simulation performed with a weak initial surface inversion layer ($\partial\vartheta_o/\partial z = 10\ \mathrm{K\,km^{-1}}$ in the lowest 1.25 km) but the same lapse rate as that in case CONTR in the mid-to-upper levels, a typical condition which occurs in the Arctic region during winter (see for example Hudak, 1994).

4.4. The "drier boundary layer" cases

Simulation results show that the development of the model frontal precipitation system is sensitive to the humidity conditions at the lower levels. Fig. 3 shows the time series of maximum frontal contrast for cases RH70 and CONTR. As

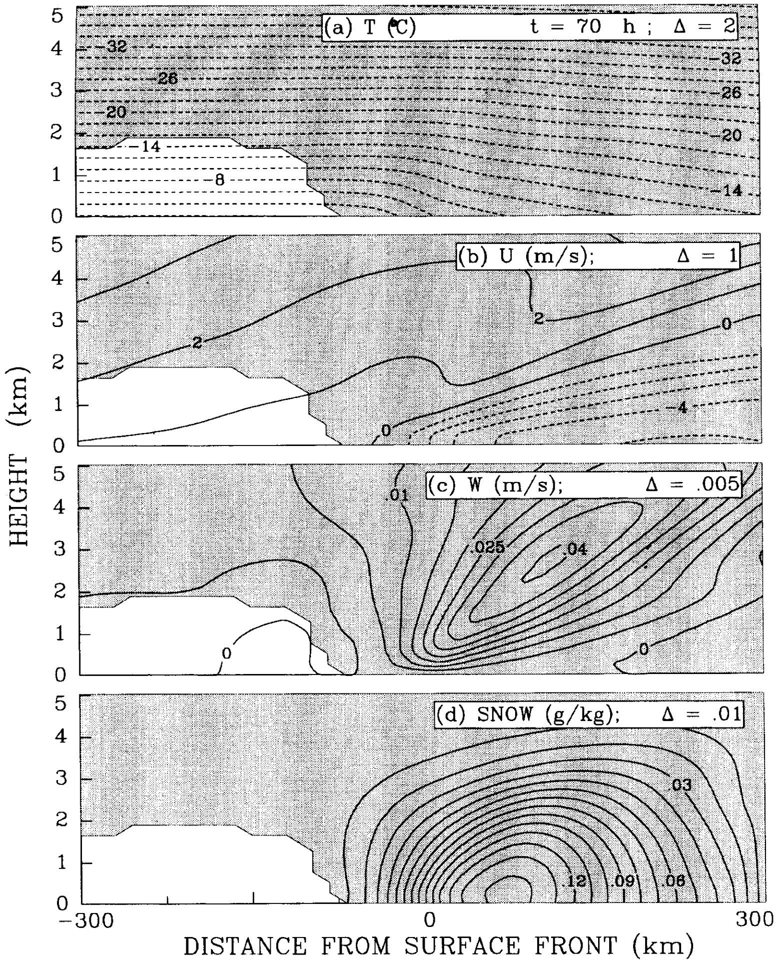

Fig. 8. As in Fig. 5 but for case MID–LAT.

expected, overall weaker frontal systems develop in the cases characterized by a drier surface layer. Less water vapor in the environment is available for condensation in the frontal uplift in these drier cases. Consequently, latent heat release is reduced and the resultant frontal circulation and hence frontogenesis is weaker than in the control case.

Fig. 9 shows the time series of the PE of model storms obtained from simulations performed with different low-level initial humidity conditions. It can be noted that non-zero PE (between 60%–70% at 70 h) was only achieved in the simulations initialized with surface RH greater than ~80%. In such cases, the PE of modelled storms compares very well to that of the observed system (60%). Therefore, the PE of the mature model storms is extremely sensitive to the low-level moisture conditions. Comparison of the results in Fig. 9 with those in Fig. 3 also shows that the drier cases do not exhibit an accelerated frontogenesis period like that found in the control case.

The zero PE in the drier lower-levels cases can be attributed to several reasons. First, the low-level moisture supply was low to begin with. Therefore, the positive feedback effects between condensational heating and frontal updraft would be reduced and enhanced frontogenesis (and the associated enhanced frontal uplift and condensation) was not possible in the drier cases during

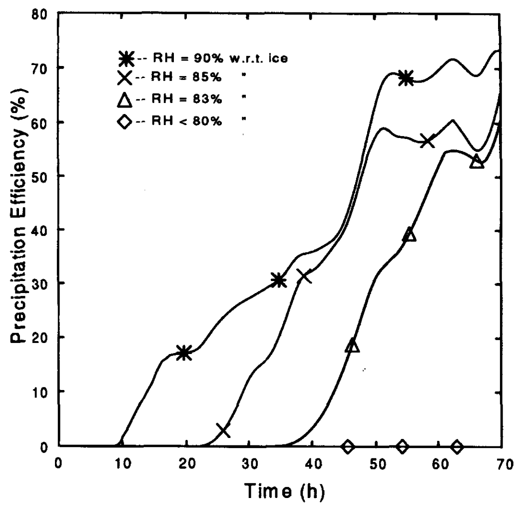

Fig. 9. Time series of the precipitation efficiency of the model storms in cases RH70-RH90.

the life-cycle of the storms. Consequently, a smaller amount of precipitation was produced which in turn made it harder to saturate the (drier) sub-cloud regions by sublimation.

PE in the mid-latitude case is also affected significantly by the low-level humidity condition as shown in the results for case MID–LAT–RH80 (Fig. 7). However, since the frontal circulation is stronger when the Coriolis parameter is reduced, more precipitation is produced in that case although a significant portion of it is lost in the sub-cloud layer. A non-zero, albeit small, PE is found in that case. Summertime mid-latitude frontal precipitation systems with deep sub-cloud layers are also often observed to possess near-zero PE (e.g., Ryan and Wilson, 1985). However, the high terminal velocities associated with raindrops suggest that the PE of such systems might not be as sensitive to the low-level moisture conditions as the winter storms studied here.

The structure of the system developed in case RH70 is shown in Fig. 10. The overall frontal structure is somewhat weaker than that in the control case. The most notable feature in the system is the total sublimational loss of snow and the associated cooling in the sub-cloud layer (Fig. 10c-d). The detrimental effect of the sublimational cooling on the frontal updraft is also evident (Fig. 10b).

4.5. *The "warm rain microphysics" case*

The time series of the PE associated the WARMRAIN case is presented in Fig. 7. It can be noted that the onset of precipitation is significantly delayed when compared to the control case. This delay in the onset of surface precipitation is related to the higher saturation vapor pressures over water than those over ice and therefore the delay in the water saturation of the model atmosphere. In addition, the coalescence of cloud particles to form raindrops is inefficient in this kind of storm environment which is characterized by weak dynamics and little moisture content. As a result, the production of precipitation in the "warm rain" case is reduced when compared to the control case. Similar results were obtained in the regional climate simulations over the Arctic region by Lynch et al. (1995).

5. Discussion

The model results presented in the previous section show that the PE of a high-latitude frontal precipitation system is very sensitive to its environmental conditions. In order to gain more insight on this problem, the various mechanisms that impact the water budget of a storm will be discussed in this section with reference to the model results.

The water budget of the model storms is governed by the following conservation equations for water vapor and condensate:

$$\frac{\partial \bar{q}_v}{\partial t} = LS_v - \bar{C} - \frac{1}{\bar{\rho}}\frac{\partial}{\partial z}\bar{\rho}\overline{w'q'_v} + Dq_v, \qquad (1)$$

$$\frac{\partial \bar{q}_c}{\partial t} = LS_c + \bar{C} - \frac{1}{\bar{\rho}}\frac{\partial}{\partial z}\bar{\rho}\overline{w'q'_c} + \bar{F} + Dq_c, \qquad (2)$$

where q_v and q_c are the mixing ratios of water vapor and liquid and ice clouds respectively, C represents the net rate of condensation, deposition, evaporation and sublimation, F is the net precipitation fallout rate, ρ is air density and w is the vertical velocity. The overbar denotes the horizontal mean and primed quantities denote the deviations from the mean. The LS terms denote large-scale convergence and the last terms (Dq_v

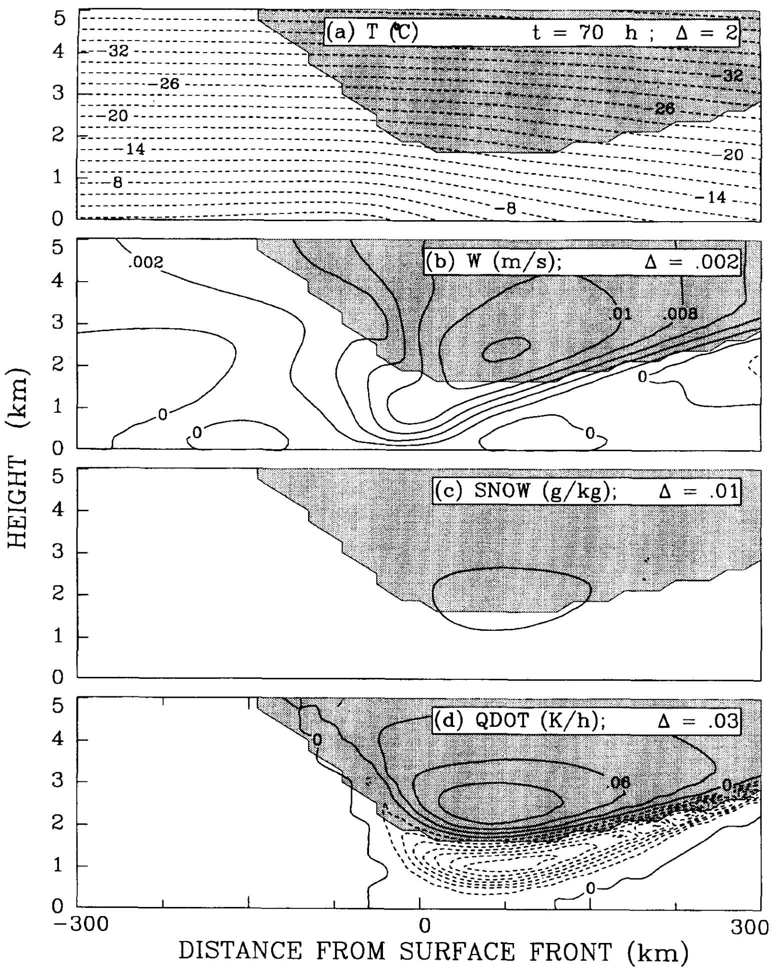

Fig. 10. Frontal structure at 70 h for case RH70: (a) temperature (b) vertical velocity, (c) snow mixing ratio and (d) heating rates.

and Dq_c) on the RHS of the equations represent subgrid-scale turbulence. Since w and therefore the vertical fluxes of q_v and q_c vanish at the lower and upper boundaries, adding the vertical integrals of (1) and (2) and neglecting the surface evaporative effects (which have not been included in the simulations presented herein), the large-scale convergence of condensates (the validity of this assumption depends on the size and location of the averaging domain and this assumption should be acceptable for the 1000 km averaging domain used in the current calculation of PE) and the turbulence effects, the following relationship for the storm water budget is produced after rearranging the terms:

$$\frac{\int \bar{\rho}\,\frac{\rho \bar{q}_v}{\rho t}\mathrm{d}z}{\int \bar{\rho} L S_v \mathrm{d}z} + \frac{\int \bar{\rho}\,\frac{\rho \bar{q}_c}{\rho t}\mathrm{d}z}{\int \bar{\rho} L S_v \mathrm{d}z} + \frac{\bar{P}_s}{\int \bar{\rho} L S_v \mathrm{d}z} = 1, \qquad (3)$$

where the P_s denotes the surface precipitation flux.

Eq. (3) states that the moisture convergence into the storm region is distributed among: (i) increasing the moisture content of the atmosphere within the storm domain (the first term on the left side of eq. (3); (ii) cloud production (the second term on the left side of eq. (3) and (iii) surface precipitation (the 3rd term on the right side of eq. (3). The 3rd term also corresponds to the definition of PE used in the previous sections.

Eqs. (1)-(3) suggest that the PE of a frontal precipitation system depends critically on several strongly coupled factors: (a) the moisture convergence into the system; (b) the vertical motion; (c) microphysical conversions inside the clouds and (d) loss of precipitation via evaporation and sublimation. Sufficient low level moisture supply by horizontal convergence and/or surface evaporation into the system is a basic requirement in the formation of cloud and precipitation on the large scale. However, the low-level moisture must be lifted sufficiently before it can condense into cloud particles.

The magnitude of frontal updraft in turn depends on several factors, namely, the background stratification, the dynamic stability of the storm environment and the frontal dynamics. The effects of varying the background static stability and planetary rotation on the frontal circulation and associated cloud and precipitation fields of the model storm have been demonstrated in the sensitivity experiments. In particular, the development of the frontal circulation and associated cloud and precipitation fields are inhibited in an environment characterized by a high Coriolis parameter and strong background stratification, conditions which are typical of the Arctic winter environment. Under such conditions the PE of the systems will be low, as shown in the model results. It should also be noted that frontal-scale dynamics are strongly coupled to the distribution of moisture in the storm environment. In particular, the convergence of moisture into the frontal region might lead to mesoscale instability (e.g., conditional symmetric instability). Under such situations, the release of instability can lead to enhanced mesoscale updraft (and thus the eddy flux divergence term in eq. (1) and increasing the PE of the system.

The condensation of water vapor into cloud particles and their subsequent growth into precipitation size particles depends critically on the microphysical properties of the storm environment (e.g., the abundance of ice and cloud condensation nuclei) and whether the storm environment is favorable for efficient precipitation production processes such as the Findeisen-Bergeron mechanism. Whether these cloud processes are represented accurately in a model will greatly affect the performance of the model. For example, results from the WARMRAIN experiment show that the onset of model surface precipitation in an Arctic winter environment will be significantly delayed when ice-phase processes are not included in the model.

If there is a significant depth of sub-saturated air below the cloud base, the precipitation produced inside the cloud will partially or totally evaporate/ sublimate in the sub-cloud layer. Due to the small terminal velocity of snow particles, the sublimation of snow is typically a much more efficient process than the evaporation of rainfall under similar conditions (Clough and Frank, 1991). The evaporation/sublimation of precipitation cools and moistens the environment. These processes will in turn lead to the sinking of the cloud base as shown in the model results (Harris, 1977). If the precipitation rate was sufficiently high or if the sub-cloud layer was not excessively dry (e.g. in the cases CONTR and MID−LAT), the cloud base might sink to be near the surface and loss of precipitation by sublimation or evaporation would become negligible and thus lead to an increase of the PE of the system. However, since the sublimation of snow is a more effective process than the evaporation of rainfall, this downward development of the cloud base will be significantly faster in storms characterized by snowfall rather than rainfall (as illustrated in the results from cases CONTR and WARMRAIN). However, the shorter residence time of rain particles in the atmosphere suggest that they might reach the surface in conditions where the snow particles might have all been sublimated in the sub-cloud layer and the PE of these systems will be less sensitive to the low level moisture conditions.

The cooling associated with sublimation/evaporation may also have significant dynamic effects on the frontal circulation. If most of the precipitation fell in the cold sector of the system, then the cooling effects could enhance frontogenesis by inducing a descent which might lead to enhanced surface horizontal convergence at the surface front (e.g., in case MID−LAT). If a significant portion of the precipitation fell into the warm sector then the cooling might have a detrimental effect on frontal uplift, thus decelerating frontogenesis and reducing condensation. These effects are reflected in the coincidence of saturation of the lower levels, the onset of the rapid frontogenetic period and the onset of the rapid growth of the PE in the control simulation. The strong sensitivity of the PE of the model storms to the low-level moisture condition is a result of these complex interacting factors.

The regional water budget depends significantly on the amount of precipitation that reaches the surface and therefore the PE of the storms occurring over the region. At least some current GCMs typically over-predict the amount of surface precipitation in high latitude regions (McFarlane et al., 1992; Bromwich et al., 1993; Lynch et al., 1995). The present results suggest that an accurate representation of cloud and precipitation processes in GCMs must account for the complex feedback between cloud microphysical processes and large-scale conditions. The cloud scheme should exhibit similar sensitivity to changes in the environmental conditions as shown in the model results before the simulated climate in the high latitudes can be improved. In addition, the model results suggest that the inclusion of ice-phase microphysics (which has typically been neglected in climate models) has great impact on the storm water budget of these Arctic systems (see also Lynch et al., 1995) and the parameterization of their effects should be improved in climate models.

6. Conclusions

A weak high-latitude warm-frontal precipitation system was simulated by using a 2D cloud-resolving model. Several important characteristics (e.g., the small horizontal scale, the steep vertical structure, extremely light snowfall and high precipitation efficiency) of the observed system were reproduced in the model. Sensitivity experiments were performed to investigate the effects of environmental conditions on the development of the system. It was found that many of the structural characteristics of the system were consequences of the sub-freezing temperatures and enhanced planetary rotation in the region.

The coupling of cloud microphysical processes to frontal scale dynamics caused the precipitation efficiency of the model storms to exhibit a strong sensitivity to low-level humidity. A high (zero) precipitation efficiency is associated with storms developed over regions having near surface relative humidity with respect to ice $\geqslant(<)80\%$. In addition, the model results show that the precipitation efficiency of the systems will be decreased (increased) when the background static stability is increased (decreased) or when the Coriolis parameter is increased (decreased).

These model results may have great implications for the water cycle as well as the parameterization of high latitude cloud systems in GCMs. For example, during the early fall when sufficient low-level moisture is still available in the region and the Arctic surface inversion layer is not well-developed, storms with high precipitation efficiency should develop over the region and act to dry out (to desiccate) the atmosphere. During the winter months when the background stratification is strong and when the low-level moisture supply is reduced (due to the frozen surface), storms with near zero precipitation efficiency should develop, no additional snow will fall over the region and the amount of vapor before and after storm development should be unchanged. The possibility that low precipitation efficiency storms may be dominant over the Arctic region during the cold season suggests then that a major portion of the water vapor converged into the region will remain in the atmosphere and that the radiation balance would consequently be affected by the ensuing clouds and water vapor in the atmosphere at a time when the production of precipitation would be minimal.

The Earth's climate is a complicated system which is comprised of many strongly coupled subsystems. The Arctic is one of the subsystems which has profound influences on the climate system. For example, all climate models predict enhanced greenhouse warming in the high latitudes (due to the ice-albedo feedback processes). If the precipitation efficiency of storms was high over the region, these systems will tend to cool and dry the environment (due to the reduced cloud coverage and precipitation cooling) and therefore offset the greenhouse effects. On the other hand, if the precipitation efficiency of the storms was low over the region (e.g., during the cold season), these storms would tend to warm and moisten the environment and therefore reinforce the greenhouse effects. In addition, it is well known that the removal by precipitation processes represents one of the major sinks for Arctic aerosols (which affects significantly the radiational budget in the Arctic region). Therefore both the concentration and distribution of aerosols in the Arctic also depend critically on the precipitation efficiency of the synoptic systems over the region. Results from high resolution cloud model simulations such as those presented in this paper will be valuable guides to the improvement of GCM model physics and to the interpretation of their simulation results. Further investigations of this subject by extending the study to include stronger Arctic systems which are often observed to develop near snow/ice edges and by using more sophisticated 3-D cloud models are warranted.

7. Acknowledgements

We wish to thank Dr. B. F. Ryan of CSIRO for his helpful comments on the manuscript. Constructive comments by the two anonymous reviewers were also much appreciated. This work was supported by the Canadian GEWEX program and the Panel on Energy Research and Development (PERD).

REFERENCES

Bannon, P. R. 1984. Effects of stratification on surface frontogenesis: warm and cold fronts. *J. Atmos. Sci.* **41**, 2021–2026.

Bluestein, H. B., 1996. Fronts and jet streaks: A theoretical perspective. In: *Mesoscale meteorology and forecasting*, P. S. Ray (ed.). American Meteorological Socicety, Boston, 173–215.

Bromwich, D. H., Robasky, R. M., Keen, R. A. and Bolzan, J. F. 1993. Modeled variations of precipitation over the Greenland ice sheet. *J. Climate* **6**, 1253–1268.

Carter, E. J. and Long, A. B. 1995. Australian Winter Storms Experiment II. Water budget, precipitation efficiency and modeling. *Preprints. Conf. Cloud Phys., 15–20 January 95. Dallas, Texas*, Amer. Met. Soc., Boston, Mass., 590 pp.

Cho, H. -R., Niewiadomski, M., Iribarne, J. V. and Melo, O. 1989. A model of the effect of cumulus clouds on the redistribution and transition of pollutants. *J. Geophys. Res.* **94**, 12 895–12 910.

Clough, S. A. and Frank, R. A. A. 1991. The evaporation of frontal and other stratiform precipitation. *Quart. J. Roy. Meteor. Soc.* **117**, 1057–1080.

Deardorff, J. W., 1971. On the magnitude of subgrid scale eddy coefficient. *J. Comput. Phys.* **7**, 120–133.

Fletcher, N. H., 1962. *The physics of rainclouds.* Cambridge University Press, Cambridge, 386 pp.

Grønås, S., Foss, A. and Lystad, M., 1987. Numerical simulations of polar lows in the Norwegian Sea. *Tellus* **39A**, 334–354.

Hanesiak, J. M., Stewart, R. E., Szeto, K. K., Hudak, D. R. and Leighton, H. G. 1997. The structure, water budget and radiational features of a high latitude warm front. *J. Atmos. Sci.*, in press.

Harris, F. I. 1977. The effects of evaporation at the base of ice precipitation layers: theory and radar observations. *J. Atmos. Sci.* **34**, 651–672.

Hobbs, P. V., Matejka, T. J., Herzegh, P. H., Locatelli, J. D. and Houze Jr., R. A. 1980. The mesocale and microscale structure and organization of clouds and precipitation in midlatitude cyclones. I: A case study of a cold front. *J. Atmos. Sci.* **37**, 568–596.

Hoskins, B. J. and Bretherton, F. P. 1972. Atmospheric frontogenesis models: Mathematical formulation and solution. *J. Atmos. Sci.* **29**, 11–37.

Houze, R. A., Locatelli, J. D. and Hobbs, P. V. 1976. Dynamics and cloud microphysics of the rainbands in an occluded frontal system. *J. Atmos. Sci.* **33**, 1921–1936.

Hudak, D. R. 1994. *A storm climatology of the southern Beaufort Sea and the Mackenzie River Delta.* Internal Report, Atmospheric Environment Service, Downsview, Ontario, Canada. 92 pp.

Kessler, E., 1969. *On the distribution and continuity of water substance in atmospheric circulation.* Meteor. Monogr., No.32, American Meteorological Society, Boston, 84 pp.

Keyser, D. and Pecnick, M. J. 1985. A two-dimensional primitive equation model of frontogenesis forced by confluence and horizontal shear. *J. Atmos. Sci.* **42**, 1259–1282.

Keyser, D. and Pecnick, M. J. 1987. The effects of along-front temperature variation in a two-dimensional primitive equation model of surface frontogenesis. *J. Atmos. Sci.* **44**, 577–604.

Lynch, A. H., Chapman, W. L., Walsh, J. E. and Weller, G. 1995. Development of a regional climate model of the western Arctic. *J. Climate* **8**, 1555–1570.

McBean, G. A. and Stewart, R. E. 1991. Structure of a frontal system over the northeast Pacific Ocean. *Mon. Wea. Rev.* **119**, 997–1013.

McFarlane, N. A., Boer, G. J., Blanchet, J. -P. and Lazare, M. 1992. The Canadian Climate Center second-generation general circulation model and its equilibrium climate. *J. Climate* **5**, 1013–1044.

Nordeng, T. E. 1990. A model-based diagnostic study of the development and maintenance mechanism of two polar lows. *Tellus* **42A**, 92–108.

Rutledge, S. A. and Hobbs, P. V. 1983. The mesoscale and microscale structure and organization of clouds and precipitation in midlatitude cyclones. Part VIII: A model for "seeder-feeder" processes in warm frontal rainbands. *J. Atmos. Sci.* **40**, 1185–1206.

Ryan, B. F. and Wilson, K. J. 1985. The Australian summertime cool change: III Subsynoptic and mesoscale model. *Mon. Wea. Rev.* **113**, 224–240.

Saarikivi, P. 1990. *Observational studies on the subsynoptic structures in extratropical cyclones.* Dept. of Meteorol., University of Helsinki, Report No. 37, 33 pp.

Saarikivi, P. and Puhakka, T. 1990. The structure and evolution of a wintertime occluded front. *Tellus* **42A**, 122–139.

Stewart, R. E., Bachand, D., Dunkley, R. R., Giles, A. C., Lawson, B., Legal, L., Miller, S. T., Murphy, B. P., Parker, M. N., Paruk, B. J. and Yau, M. K. 1995a. Winter storms over Canada. *Atmos. Ocean.* **33**, 223–247.

Stewart, R. E., Yiu, D. T., Chung, K. K., Hudak, D. R., Lozowski, E. P., Oleskiw, M., Sheppard B. E. and Szeto, K. K. 1995b. Weather conditions associated with the passage of precipitation type transition regions over Eastern Newfoundland. *Atmos. Ocean.* **33**, 25–53.

Szeto, K. K. and Cho, H. -R. 1994. A numerical investigation of squall lines. Part I. The control experiment. *J. Atmos. Sci.* **51**, 414–424.

Szeto, K. K. and Stewart, R. E. 1997. Effects of melting on frontogenesis. *J. Atmos. Sci.* **54**, 689–702.

Tanguay, M., Robert, A. and Laprise, R. 1990. A semi-implicit fully compressible regional forecast model. *Mon. Wea. Rev.* **118**, 1970–1980.

Washington, W. M. and Meehl, G. A. 1996. High-latitude climate change in a global coupled ocean-atmosphere-sea ice model with increased atmospheric CO_2, *J. Geophys. Res.* **101**, D8, 12795–12801.